DOE/ER/10361--12

DOE/ER/10361--T2

DE83 015143

EFFECTS OF WATER-SATURATION ON STRENGTH AND DUCTILITY OF THREE IGNEOUS ROCKS AT EFFECTIVE PRESSURES TO 50 MPA AND TEMPERATURES TO PARTIAL MELTING

S. J. Bauer, M. Friedman, and J. Handin

Center for Tectonophysics
Texas A&M University
College Station, TX 77843

INTRODUCTION

Energy extraction from the geothermal regime in and above buried magma-chambers requires that rocks be drillable (brittle or semi-brittle) and boreholes be stable to depths of 10 km, at temperatures to partial melting, and in a natural or manmade aqueous environment. Critical are the short-term strengths and ductilities that would govern during and immediately after drilling, and the longer-term, time-dependent response, that would influence the stability of a borehole over the multi-year life-expectancy of a geothermal well.

At least initially, we chose to investigate the short-term failure strengths and strains at failure of room-dry and water-saturated, cylindrical specimens (2 by 4 cm) of Charcoal Granodiorite (CG), Mt. Hood Andesite (MHA), and Cuerbio Basalt (CB) at a strain rate of $10^{-4}s^{-1}$, at effective confining pressures of 0, 50, and 100 MPa and at temperatures to partial melting. Previous laboratory work needed to be augmented because virtually all testing above 500°C had been done at either atmospheric pressure (e.g., Murrell and Chakravarty, 1973), at too high a confining pressure (e.g., Handin, 1966; Carter, 1976; Tullis and Yund, 1977; Carter and Kirby, 1978; Tullis, 1979), or at uncertain effective pressures (e.g., Murrell and Ismail, 1976; Tullis and Yund, 1978; Van der Molen and Paterson, 1979). Available data on creep of crystalline rock have suggested that deformation rates are very slow even at elevated temperatures and pressures (Carter and Kirby, 1978; Handin and Carter, 1980; and Carter et al., 1981). Only when partial melting occurs do rock-strengths vanish and relatively low viscosities obtain (Van der Molen and Paterson, 1979; Friedman et al., 1980). Hence our emphasis is on the short-term effects. Previously we dealt with room-dry specimens of these three rocks and with the Newberry Rhyolite Obsidian (Friedman et al., 1979, 1980). This was necessary because "dry-out" zones may exist immediately above buried magma and a data-base for dry rocks is needed for comparison with water-saturated counterparts in order to distinguish between effective pressure and water-weakening effects. Herein we report on experiments on the water-saturated specimens.

APPARATUS AND PROCEDURES

The triaxial-compression apparatus, including the hydraulic press and internally-heated pressure cell, the starting materials, sample preparation, and plotting of true axial differential stress (MPa) against conventional strain (percent shortening) are fully described in previous publications (Friedman et al., 1979, 1980). The accuracy of measurements of differential force, shortening, external confining pressure (P_c), and internal pore pressure (P_p) is of the order of $\pm$ 2 percent. Temperature (T) is known within $\pm$ 5°C, and the maximum gradient along the length of the specimen is 30°C at 1000°C nominal. In brief, (1) the 2 by 4-cm cylindrical specimens are vacuum-saturated with tap water and stored under water until they are jacketed in thin-walled, annealed copper tubes and emplaced within the internal furnace of the test cell; (2) a small axial force is applied to seat and seal off the specimen and the cell is purged of air and filled with the confining medium of argon; (3) the axial force, external confining pressure, and internal pore pressure are raised simultaneously to the desired effective confining pressure, $P_e = P_c - P_p$; (4) the specimen is heated to test temperature at about 10°C/min; (5) the specimen is soaked for 15 min, effective confining pressure and temperature being readjusted if necessary (increasing soak-time to 1 hour does not significantly affect the results); (6) the specimen is loaded axially such that $\sigma_1 > \sigma_2 = \sigma_3 = P_e$, where σ_i are the effective principal compressive stresses, P_e remaining sensibly constant because strains before macroscopic fracture are small, only about 1 percent.

Using the laboratory data to predict borehole stability where $\sigma_1 > \sigma_2 > \sigma_3$, we shall assume that ultimate compressive strength at failure, the peak value of the differential stress, $\sigma_1 - \sigma_3$, at a particular temperature, is a function only of mean stress, $\sigma_m = (\sigma_1 + \sigma_2 + \sigma_3)/3$. Thus for each test we compute $(\sigma_1 - \sigma_3)$ and σ_m and list them together with the total shortening at macroscopic failure that serves as a measure of relative ductility (Table 1). We also show the angle θ between the load axis (σ_1) and the macroscopic fault.

EXPERIMENTAL RESULTS

The experimental data on Charcoal granodiorite, Cuerbio basalt, and Mt. Hood andesite are listed in Table 1. All tests were done at a nominal strain-rate of 10^{-4}/s, and all were stopped short of total loss of cohesion of the deformed specimens. Stress-shortening curves are similar to those published previously (Friedman et al., 1979, 1980). Those for the CG show well defined ultimate strengths at <2% shortening and then pronounced work-softening as slip occurs along faults. Those for the MHA exhibit ultimate strengths at $\leq$3% shortening, and quasi-steady-state, ductile flow, particularly at the higher temperatures where partial melting occurs. The plots of ultimate strength versus temperature for the water-saturated rocks are compared with their counterparts for dry specimens (Figures 1, 2, 3).

Charcoal Granodiorite

At zero effective confining pressure ($P_c = P_p = 0$ or $P_c = P_p = 50$ MPa) strength decreases gradually with increasing temperature until it vanishes at

DISCLAIMER

about 1050°C where partial melting is pervasive (Figure 1). The reproducibility of duplicate tests under the same conditions is regarded as relatively good for triaxial testing of statistically homogeneous and isotropic rocks like the granodiorite. The strengths of dry and water-saturated specimens are virtually identical at 400° and 1015°C; wet specimens are somewhat the stronger in the range of 460° to 990°C.

At 50-MPa effective pressure (P_c = 50, P_p = 0 or P_c = 100, P_p = 50) the rock is much stronger at all temperatures. Reproducibility is generally only fair, but the strengths of wet specimens at 800° and 810°C are virtually identical, and the strengths of all wet specimens in the range of 615° to 900°C lie close to those of dry specimens at P_e = 50 and far below those at P_c = P_e = 100 MPa, suggesting that pore pressures must be nearly fully effective.

The presence of water does not significantly affect either strength or ductility. All specimens are essentially brittle, failing by macroscopic shear fracturing at strains of the order of 1 percent (Table 1).

Mt. Hood Andesite

This rock is finer-grained but more porous and permeable that the CG, and its matrix contains minor amounts of glass. It is much weaker than the granodiorite at all effective pressures and temperatures. At P_c = P_p = 0, the strength of the dry andesite remains nearly constant as temperature is increased from 25° to 1000°C, but suddenly vanishes at about 1050°C (Figure 2). Reproducibility of tests is regarded as good. The strengths of dry and of wet specimens at P_c = P_p = 50 MPa are identical at 615°C, but the wet andesite is much the weaker at 700°C, and its strength vanishes when partial melting occurs, unlike that of the granodiorite. The melting temperature for this rock is reduced >150°C by the presence of water.

At the higher 50-MPa effective confining pressure (P_c = 50, P_p = 0 or P_c = 100, P_p = 50) this rock is much stronger at all temperatures. Again contrary to the behavior of the granodiorite, the strength of wet andesite in the range of 600° to 920°C lies well below that of the dry rock and far below that at P_c = 100, P_p = 0. Furthermore, the strains at failure of the wet specimens are somewhat the larger.

Cuerbio Basalt

Relatively few data are available for this dense, tight rock, but the effects of water saturation are still evident (Figure 3). The strengths of the dry rock at P_c = 0 is little affected by heating from 25° to 900°C. At P_c = 50, the strength drops from about 500 MPa at 25°C to about 350 at 600° to about 100 at 1000°C. At P_c = 100, it drops from 465 at 700° to 180 at 1000°.

The strength of the water-saturated basalt at zero effective confining pressure (P_c = P_p = 50 MPa) is much like that of the dry rock to about 750°C; above 800° it drops rapidly to 60 MPa at 945°. The basalt too is essentially brittle at all pressures and temperature (Table 1).

Mechanism of Deformation

As noted in Table 1 most of the water-saturated rock specimens are macroscopically shattered, i.e., they failed along two or more shear fractures or faults. This often gives rise to an apparent steady-state or work-softening stress-shortening curve. Crystal plastic flow is conspicuous only in favorably oriented, kinked biotite. True ductile flow occurs with incipient melting. In its very incipient stages this melting occurs at grain boundaries associated with biotite or hornblende, within feldspar and quartz grains as manifest by isolated patches of vesicules, or along fractures similar to that found by Van der Molen and Paterson (1979).

Aside from the incipient melting, microfracturing and the coalescence of microcracks into the macroscopic faults are the major mechanisms of deformation. Quantitative assessment of the abundance of these microfractures in wet tests shows that they are not more abundant than in dry counterparts. That is, about the same number of microfractures occurs prior to failure, wet or dry.

MECHANISMS FOR WATER-WEAKENING

Water-weakening can owe to (a) chemisorption or stress corrosion effects at crack tips that reduce fracture strengths (e.g., review by Anderson and Grew, 1977), (b) lowered melting points, and (c) lowering of the critical resolved shear stresses for dislocation gliding, i.e., yield strengths for crystal-plastic mechanisms (e.g., Griggs and Blacic, 1965; Griggs, 1974; Balderman, 1974; Tullis, 1979). All three effects involve hydration of the silanol bonds in silicates. The higher is the temperature, the more significant is this phenomenon likely to be (Griggs, 1967). Without detailed thin-section and perhaps TEM studies (scheduled for the future), we can not say which of these mechanisms has lowered the strength of the andesite at elevated temperatures, but it is generally recognized that H_2O must gain access to the crystal surfaces (item a, above) and then to their substructures (items b and c, above) to effect the hydrolytic weakening. It is not surprising therefore, that of the three rocks tested, the andesite shows the greatest weakening probably because its relatively larger porosity (10-12 percent) allows greater access of the pore water to its internal surfaces.

In the ductile regime temperature (300-500°C) affects the water-weakening of quartz (Griggs, 1967; Balderman, 1974). Our maximum temperatures much exceed these. More recently however, a pressure effect has been found, as water is driven from the surfaces of pores and cracks into the adjacent crystal structures at high pressure (Tullis, 1979). Our pore pressures (50 and 100 MPa) are small compared to those (1000 and 1500 MPa) needed in the laboratory to achieve this effect (Tullis and Yund, 1978), so that water-weakening (item c, above) is not expected. Instead, the brittle response of our specimens suggests that the water-weakening of the andesite is due to stress-corrosion and/or the reduced melting temperature. This view is supported by the microfracture-abundance data which indicate that the same number of microfractures form regardless of water-content. This number appears to be critical for failure, and when the specimen is water-weakened this critical assemblage of fractures is

obtained at a lower externally imposed differential stress. Thus, local fracture strengths must be reduced in the presence of water.

PARTIAL MELTING

In our water-saturated tests only incipient stages of partial melting have been obtained with <3 percent glass found along grain boundaries and axial fractures in CG specimen 308 and MHA specimens 297, 305, 312, and 325 (Table 1). Our results differ from those of Van der Molen and Paterson (1979) on a fine-grained quartz monzonite in two important ways. They observe (1) more partial melting than we do at 800°C; and (2) a gradual decrease in strength from about 250 MPa at 5 percent melt to about 60 MPa at 15 percent melt, and then a drop to <1 MPa at 24 percent melt. In contrast we find larger strength reductions from much smaller amounts of melt. The first result probably obtains because their specimens are "soaked" at P and T for 100 minutes prior to shortening (as opposed to 15 minutes for ours) and their strain-rate ($10^{-5}s^{-1}$) is one order of magnitude slower than ours. We have no ready explanation for the second result because their effective pressures are unknown.

BOREHOLE STABILITY

The rationale for our simplistic scheme to predict borehole stability is detailed by Friedman et al. (1979, 1980). In brief, (1) the experimental ultimate differential stress and mean stress at failure for each rock are plotted in three (Figure 4) or two dimensions (Figure 5). (2) Purely mechanical borehole-stresses are calculated from elastic theory with certain assumptions about the far-field stresses (σ_h equal in all directions and σ_h/σ_v = 2, 1, or 0.5), borehole filling (open or filled with a material with the density of 1.0 g/cc) and the water content of the rock (dry or saturated) (Friedman et al., 1979, Table 6). (3) The borehole stresses as a function of depth are then drawn as surfaces in three dimensions or straight lines (loci) on the plots containing the failure data (Figures 6 and 7, respectively). (4) In order to use the laboratory data to predict failure of a borehole, we assume that ultimate strength (σ_1-σ_3) at failure is a function only of the effective mean stress, $\sigma_m = (\sigma_1 + \sigma_2 + \sigma_3)/3$ and temperature. (5) If at a given mean pressure, say 50 MPa, the strengths for a given rock exceed the borehole differential stress, then the borehole will be stable. That is, it will not fail by shear fracturing in the short term. (6) Intersections of lines connecting strength data for a given temperature and the borehole-stress loci mark the boundaries between the fields of stability, containing all points to the left of the loci of borehole stresses, and of instability, containing all points to the right. Stated another way, the borehole will fail if the borehole-stress-loci intersect the failure surface (Figure 4). Predictions based on the dry strengths of all three rocks are given in Friedman et al. (1979, 1980).

Here we concentrate on the likelihood of stable boreholes in water-saturated CG and MHA (Figures 7 and 8, respectively). The available data indicate (1) both rocks would afford stable boreholes to >10 km if σ_h/σ_v were 1.0 and the boreholes were filled with a material of density 1.0 g/cc; (2) boreholes in CG would be stable to >10 km at all assumed conditions provided that the temperature did not exceed about 800°C; (3) boreholes would be much less stable in the water-weakened MHA, and depending upon the far-field conditions would fail at 700°C at depths ranging from 2 to 5 km; and (4) boreholes even in the MHA would be stabilized appreciably if kept cool $\leq$ 700°C.

We have addressed the matter of short-term borehole stability. They do not consider time effects, irregularities at the borehole wall that would concentrate the stresses and enhance failure, or existing natural fractures. Nor have we treated superposed thermomechanical stresses arising from cooling a borehole in hot country rock. These would tend to diminish the differential stresses at the borehole wall and so promote stability.

CONCLUSIONS

Data from water-saturated specimens of the granodiorite and andesite, compared to room-dry counterparts, indicate (1) the pore pressures are essentially communicated throughout each test specimen so that they are fully effective; (2) at P_e = 0 and 50 MPa [P_c and P_p of 50 MPa and of 100 and 50 MPa, respectively] the granodiorite does not water-weaken; (3) at these same effective pressures the more porous and finer-grained andesite begins to exhibit water-weakening at about 600°C; (4) at P_e = 0 and 870-900°C the andesite's strength averages 20 MPa while the strength of dry specimens at the same P and T exhibit a strength of 100 MPa, i.e., strength is reduced by a factor of 5; (5) at P_e = 50 MPa and 920°C the andesite's wet strength is 45 MPa compared to 160 MPa dry; (6) the basalt at P_e = 0, appears to be water-weakened at 800°C; (7) ductility of the water-saturated specimens deformed at temperatures less than that of melting exhibit ultimate strengths at less than 2 percent shortening and then work-soften along faults, i.e., like their dry counterparts the rocks remain brittle up to the onset of melting; (8) again as do the dry counterparts, the wet specimens deform primarily by microscopic fracturing that coalesces into one or more macroscopic faults; and (9) the temperature for incipient melting of the andesite is decreased >150°C in the water-saturated tests.

Extrapolations of strength and ductility data for both wet and dry specimens indicate: (1) crystalline rocks should be drillable because they remain brittle until partial melting occurs, and penetration rates should increase with temperature because of a corresponding decrease in brittle fracture strength; (2) boreholes in "water-filled" holes should be stable to >10 km at temperatures <T_m; (3) if temperatures are kept to $\leq$700°C, even open boreholes in granodiorite are apt to be stable to >10 km; and (4) open boreholes in the andesite would be much less stable, and at similar temperatures would fail at 2 to 5-km depth. Work to date on intact specimens suggests it is scientifically feasible to drill to buried magma chambers at depths to 10 km. Boreholes can be stabilized by keeping them as cool as possible and subject to a borehole pressure equivalent to that of a column of water at 25°C.

ACKNOWLEDGMENTS

This work was supported by the Office of Basic Energy Sciences, Department of Energy, Contract No. DE-AS05-79-ER10361.

REFERENCES

Anderson, O. L., and P. C. Grew, 1977, Stress corrosion theory of crack propagation with applications to geophysics, Review of Geophysics and Space Physics, Vol. 15, pp. 77-104.

Balderman, M. A., 1974, The effect of strain rate and temperature on the yield point of hydrolytically weakened synthetic quartz, Journal of Geophysical Research, Vol. 79, pp. 1647-1652.

Carter, N. L., 1976, Steady state flow of rocks, Review of Geophysics and Space Physics, Vol. 14, pp. 301-357.

Carter, N. L., and S. H. Kirby, 1978, Transient creep and semibrittle behavior of crystalline rocks, Pure and Applied Geophysics, Vol. 116, pp. 806-839.

Carter, N. L., D. A. Anderson, F. D. Hansen, and R. L. Kranz, 1981, Creep and creep-rupture of granitic rocks, in The Handin Volume, American Geophysical Union, Geophysical Monograph Series, in press.

Friedman, M., J. Handin, N. G. Higgs, and J. R. Lantz, 1979, Strength and ductility of four dry igneous rocks at low pressures and temperatures to partial melting, Proceedings of the 20th U.S. Symposium on Rock Mechanics, Austin, pp. 35-50.

Friedman, M., J. Handin, N. G. Higgs, J. R. Lantz, and S. J. Bauer, 1980, Strength and ductility of room-dry and water-saturated igneous rocks at low pressures and temperatures to partial melting, Sandia Laboratories, Final Report Contract No. 13-2242, 86 p.

Griggs, D., 1967, Hydrolytic weakening of quartz an other silicates: Geophysical Journal of the Royal Astronomical Society, Vol. 14, pp. 19-31.

Griggs, D., 1974, A model of hydrolytic weakening in quartz: Journal of Geophysical Research, Vol. 79, pp. 1653-1661.

Griggs, D. and J. D. Blacic, 1965, Quartz: Anomalous weakness of synthetic crystals: Science, Vol. 147, pp. 292-295.

Handin, J., 1966, Strength and ductility, Section 11, in Handbook of Physical Constants, Revised Edition, Geological Society of America Memoir 97.

Handin, J., and N. L. Carter, 1980, Rheological properties of rocks at high temperatures, in Proceedings of the 4th Congress International Society of Rock Mechanics, Vol. 3, Montreux, Switzerland, pp. 97-106.

Murrell, S. A. F., and S. Chakravarty, 1973, Some new rheological experiments on igneous rocks at temperatures up to 1120°C, Geophysical Journal of the Royal Astronomical Society, Vol. 34, pp. 211-250.

Murrell, S. A. F., and I. A. H. Ismail, 1976, The effect of temperature on the strength at high confining pressure of granodiorite containing free and chemically-bound water, Contributions Mineralogy Petrology, Vol. 55, pp. 317-330.

Tullis, J. A., 1979, High temperature deformation of rocks and minerals, Reviews of Geophysics and Space Physics, Vol. 17, pp. 1137-1154.

Tullis, J., and R. A. Yund, 1977, Experimental deformation of dry Westerly granite, Journal of Geophysical Research, Vol. 82, pp. 5705-5718.

Tullis, J. A. and R. A. Yund, 1978, Water-weakening of experimentally deformed Westerly Granite: Journal of Geophysical Research, Vol. 82, pp. 5705-5718.

Van der Molen, I., and M. S. Paterson, 1979, Experimental deformation of partially-melted granite, Contributions Mineralogy Petrology, Vol. 70, pp. 299-318.

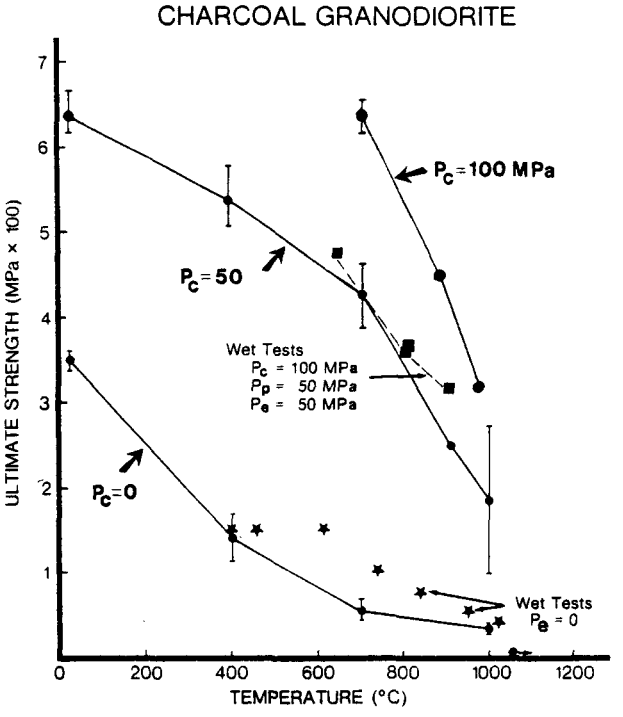

Figure 1. Ultimate strength versus temperature for Charcoal Granodiorite. Solid circles show data points at confining pressures of 0, 50, and 100 MPa for room-dry specimens. Solid stars and squares show data points for water-saturated specimens at P_e of 0 and 50 MPa, respectively.

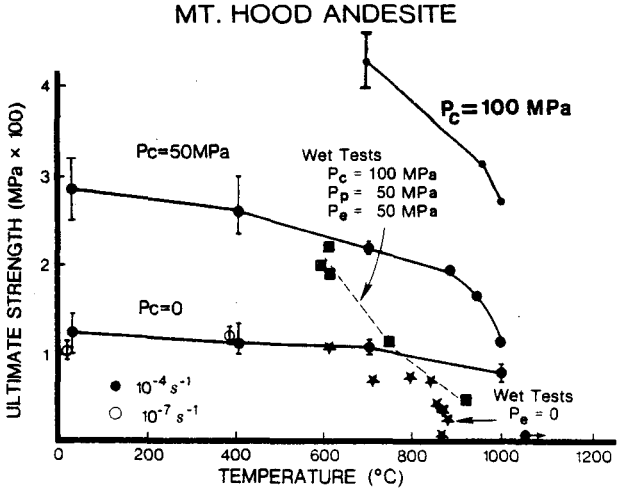

Figure 2. Ultimate strength versus temperature for Mt. Hood Andesite. Solid circles show data for room-dry specimens at confining pressures of 0, 50, and 100 MPa. Stars and squares show data for water-saturated specimens at P_e of 0 and 50 MPa, respectively.

Table 1. Experimental Data for Water-Saturated Charcoal Granodiorite, Cuerbio Basalt and Mt. Hood Andesite Shortened at 10^{-4} s^{-1}.

Rock Type and Specimen No.	Confining Pressure (MPa)	Pore Pressure (MPa)	Effective Pressure (MPa)	Temp. (°C)	Mean Stress (MPa)	Ultimate Strength (MPa)	Shortening at Failure (%)	
CHARCOAL GRANODIORITE								
280	100	100	0	400	50	150	0.7	Shattered, work-softened to 50 MPa at 1.9% shortening.
286	50	45	5	460	50	150	-	θ = 23°, } Heated at differential stress of 150 MPa until specimen failed.
287	50	45	5	610	50	150	-	Shattered)
289	50	50	0	740	35	100	1.0	Shattered, work-softened along multiple fractures to 45 MPa at 2.7% shortening.
291	50	50	0	835	25	75	1.0	θ = 34°, work-softened along fault to 15 MPa at 2.5% shortening.
294	50	50	0	945	20	55	0.9	θ = 34°, work-softened along fault to 15 MPa at 2.1% shortening, no melting.
308	50	50	0	1015	15	40	0.6	Shattered, work-softened along fault to 25 MPa at 3.2% shortening, partially melting.
311	50	50	0	990	15	40	0.4	Shattered.
320	100	50	50	615	210	485	1.3	θ = 27°.
314	100	50	50	800	170	360	1.7	Shattered, θ = 36° (best fault).
317	100	50	50	900	155	315	1.6	Shattered, θ = 34° (best fault).
324	100	50	50	810	174	372	1.5	Shattered, specimen held at T = 810°C 45 minutes prior to application of differential stress.
CUERBIO BASALT								
296	50	50	0	415	85	255	0.6	Shattered, work-softened along multiple fractures to 115 MPa at 1.7% shortening.
304	50	50	0	765	80	235	0.8	Shattered, work-softened with stick-slip to 135 MPa at 2.5% shortening.
307	50	50	0	916	30	90	0.9	Shattered, work-softened along multiple fractures to 60 MPa at 3.4% shortening.
309	50	50	0	850	45	135	0.3	Shattered.
310	50	50	0	945	20	60	0.1	Shattered, work softened along multiple fractures to 45 MPa at 2.7% shortening.
318	100	50	50	820	110	180	1.0	Shattered, θ = 35° (best fault)
MT. HOOD ANDESITE								
306	50	50	0	615	35	105	0.6	Shattered, work-softened along multiple fractures to 25 MPa at 1.8% shortening.
290	50	50	0	720	25	70	0.6	Shattered, work-softened along multiple fractures to 25 MPa at 2.0% shortening.
300	50	50	0	800	25	70	0.6	Shattered, work-softened along multiple fractures to 20 MPa at 3.5% shortening.
301	50	50	0	845	20	65	0.8	Shattered, work-softened along multiple fractures to 15 MPa at 4.0% shortening.
302	50	50	0	855	15	40	0.8	Shattered, work-softened along multiple fractures to 15 MPa at 4.3% shortening.
303	50	50	0	870	10	35	0.8	Shattered, work-softened along multiple fractures to 20 MPa at 3.1% shortening.
297	50	50	0	870	0	5	1.0	Ductile, no fracturing or faulting, total shortening 2.8% before test stopped.
305	50	50	0	880	10	25	0.7	Shattered, work-softened along multiple fractures to 10 MPa at 2.5% shortening, incipient melting (?)
327	100	50	50	600	120	205	1.5	Shattered, work-softened along multiple fractures to 195 MPa at 3.5% shortening.
319	100	50	50	610	125	225	2.0	Shattered, work-softened along multiple fractures to 215 MPa at 4.1% shortening.
324	100	50	50	610	115	190	3.2	Shattered, work-softened along multiple fractures to 190 MPa at 3.2% shortening.
312	100	50	50	745	85	110	3.4	Ductile, no faults to 3.5% shortening incipient melting.
325	100	50	50	920	65	45	3.1	Ductile, no faults to 3.3% shortening incipient melting.

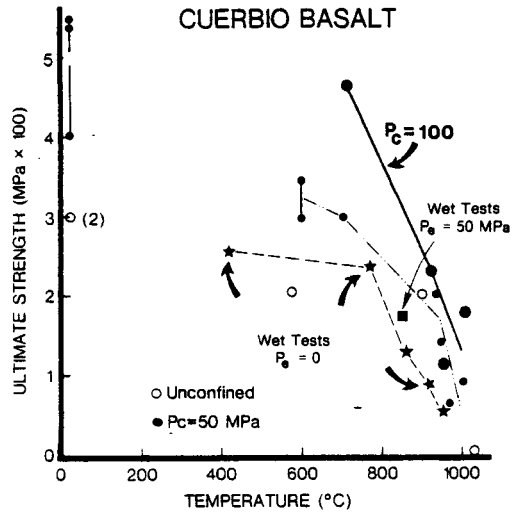

Figure 3. Ultimate strength versus temperature for Cuerbio Basalt. Solid and open circles show data for room-dry specimens at confining pressures of 0, 50, and 100 MPa. Solid stars and squares show data for water-saturated specimens at P_e = 0 and 50 MPa, respectively.

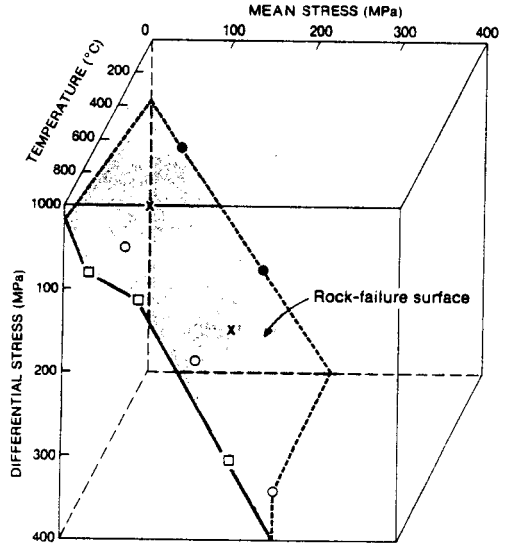

Figure 4. Failure surface for room-dry MHA in three dimensions to be compared with similar data plotted in two dimensions (Figure 5). Differential and mean stress are plotted for 25° (solid dot), 400° (cross), 700° (open circle), and 960-1000° (open square).

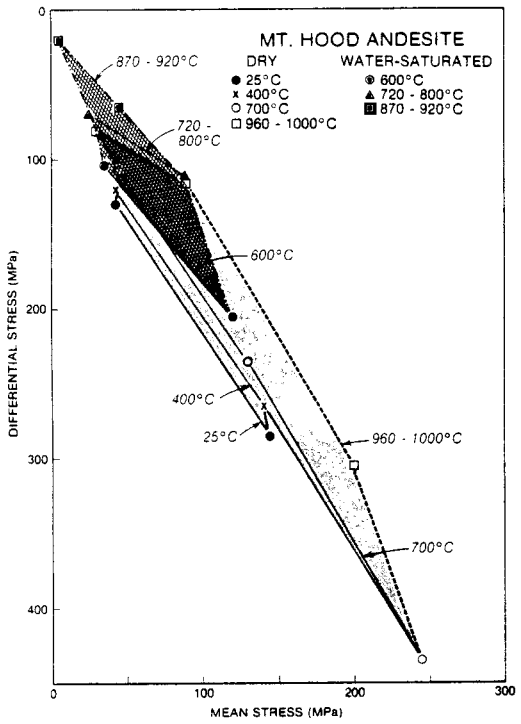

Figure 5. Failure surfaces for room-dry (light gray) and water-saturated (cross-hatched) specimens of Mt. Hood Andesite. Water-weakening has translated the failure surface upwards toward lower mean- and differential-stress levels.

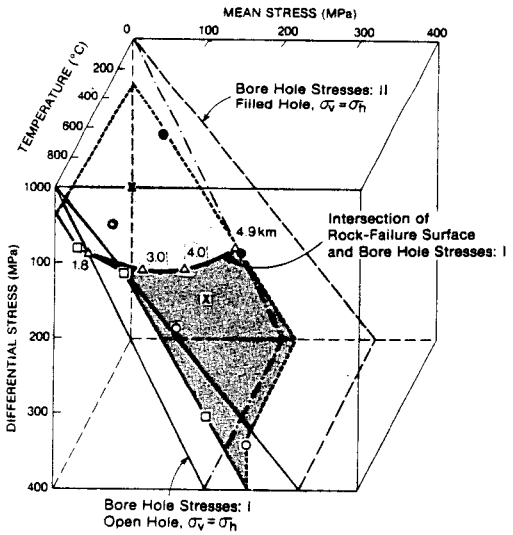

Figure 6. Diagram shows in three dimensions the failure surface for room-dry Mt. Hood Andesite and two sets of borehole stresses (I and II). Failure surface intersects only one loci of borehole stresses (I) at depths of 4.9, 4.0, 3.0, and 1.8 km for temperatures of 25°, 400°, 700°, and 960-1000°C, respectively. These depths are determined from the gradient of the borehole stresses, which is fixed for each set of assumptions.

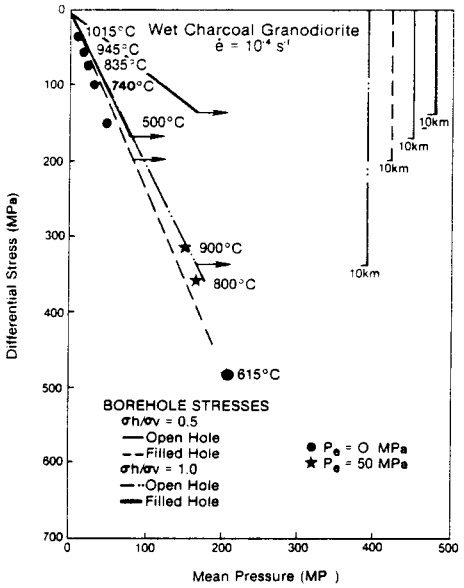

Figure 7. Assessment of borehole stability in water-saturated Charcoal Granodiorite at P_e of 0 (solid dots) and 50 MPa (solid stars). Temperatures correspond to data located immediately to left. Four borehole-stress loci and their corresponding depth scales are given. Failure is expected when a line connecting data for a given temperature intersects a borehole stress locus.

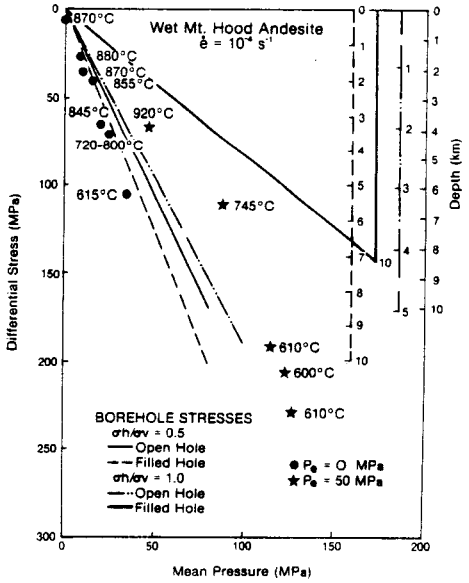

Figure 8. Assessment of borehole stability in water-saturated Mt. Hood Andesite at P_e = 0 (solid circles) and 50 MPa (solid stars). Details are same as those in Figure 7.

DISCLAIMER